

# Investigation of pore initiation in metal foams by synchrotron-radiation tomography

L. Helfen,<sup>a)</sup> T. Baumbach, and P. Pernot

*Institut für Synchrotronstrahlung (ISS/ANKA), Forschungszentrum Karlsruhe, D-76344 Eggenstein-Leopoldshafen, Germany*

P. Cloetens

*European Synchrotron Radiation Facility (ESRF), F-38043 Grenoble, France*

H. Stanzick

*Fraunhofer Institute for Manufacturing and Advanced Materials (IFAM), D-28359 Bremen, Germany*

K. Schladitz

*Fraunhofer Institute for Industrial Mathematics (ITWM), D-67663 Kaiserslautern, Germany*

J. Banhart

*Hahn-Meitner-Institut (HMI), D-14109 Berlin, Germany*

(Received 13 December 2004; accepted 25 April 2005; published online 1 June 2005)

Synchrotron-radiation tomography was used to investigate early foaming stages of aluminium alloys. Monochromatic radiation, high spatial resolution down to the micrometer scale, partial beam coherence, and holographic reconstruction techniques permit the distinction between different foam constituents which are not visible by other volume imaging techniques. In combination with three-dimensional image analysis, the differences in the pore initiation processes in two different aluminium alloys are shown. We find that, in powder compacts made from prealloyed AA6061 alloy powder, pores appear predominantly around the blowing agent particles whereas, in compacts made from a powder blend of Al and Si, pores tend to initiate around Si particles. © 2005 American Institute of Physics. [DOI: 10.1063/1.1941453]

Aluminium foam is a good candidate for a wide range of engineering applications owing to its low specific weight and good energy-dissipation properties.<sup>1,2</sup> A growing number of companies is producing such foam for various applications.<sup>3</sup> One of the most promising production methods for metal foams is known as the *powder-compact* or *powder-metallurgical* route:<sup>4</sup> Foams are produced by subjecting a foamable precursor material to a heat treatment above the melting temperature of the metal. The precursor is a powder-compact containing a blowing agent which—above its decomposition temperature—releases a blowing gas (usually hydrogen), thus inflating pores in the formerly almost dense precursor material. In contrast to processes in which foams are prepared by gas injection into a liquid, the first formation of pores during foaming of a solid precursor can already take place before any liquid occurs. Naturally, in this stage, growth of pores is governed by solid-state properties, whereas surface tension becomes dominant in later stages after melting.

Although there has been intense research activity for many years, the formation of metal foams is only partly understood up to now. Nondestructive imaging methods such as x-ray radiography and tomography already provided valuable information about microstructural evolution during metal foam formation. Real-time synchrotron-radiation (SR) radiography enabled imaging of the entire foaming process *in situ*,<sup>5,6</sup> monitoring the initiation of oblate cracks rather than round spherical pores for a wide range of Al alloys. However, radiography is not able to provide three-dimensional (3D) structural properties including 3D statisti-

cal analysis. Structural studies of metal foams by laboratory tomography until now focused on expansion states near full expansion (see, e.g., Refs. 7,8) at spatial resolutions around 10  $\mu\text{m}$ .

It is still not clear, where cracks initiate in the solid state during foam expansion. Formation in the vicinity of the blowing agent particle has been postulated as well as at locations of structural weakness.<sup>9</sup> The observed differences in the foaming behavior of different aluminium alloys suggest that the mechanisms might vary. Cracking at spatial inhomogeneities could lead to networks of cracks<sup>10</sup> which facilitate the blowing gas to escape from the solid matrix and thus retard foam expansion which is a potential technological drawback.

So far, the investigation of pore initiation was limited to *ex situ* surface examination of foam samples by scanning electron microscopy (SEM) and metallography.<sup>11</sup> Due to destructive sample preparation (cutting, polishing, etc.) such 2D surface investigations may lead to a false interpretation.<sup>9</sup> For example, the polishing can remove constituting particles (e.g., of the blowing agent) from the surface or particles can be hidden in deep pores which cannot be investigated from the surface.

Therefore, nondestructive 3D investigation methods are of crucial importance to provide reliable information about the microstructural constituents and their spatial correlation. For this reason we applied SR tomography<sup>12-14</sup> with down to micrometer resolution and in both the absorption-contrast and holographic imaging modes to solve these questions.

We employed the microtomography setup of beamline ID19 at the ESRF (see Fig. 1). At four detector-sample distances (4, 64, 154, and 400 mm), tomographic scans of each

<sup>a)</sup>Electronic mail: helfen@esrf.fr

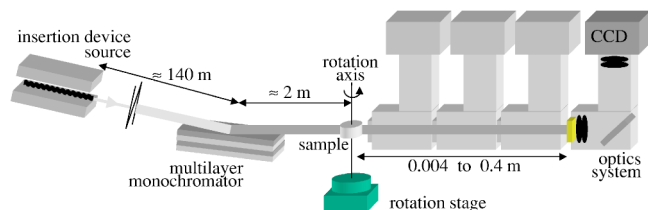


FIG. 1. Sketch of the experimental setup for holographic tomography at beamline ID19 of the ESRF. Radiographs exhibiting interference patterns due to Fresnel diffraction are recorded at different distances to the sample.

1400 projections were acquired at an x-ray energy of 18 keV and using a detector pixel size of  $1.4 \mu\text{m}$ . Absorption tomography—based on the attenuation of x rays by a sample—is carried out at the smallest detector-sample distance, providing the 3D distribution of the linear attenuation coefficient  $\mu(\vec{x})$  after reconstruction by a filtered-backprojection algorithm for the parallel-beam case. By combining the information obtained at the four different distances, holographic phase-contrast tomography<sup>14,15</sup>—enabled by a high spatial coherence (transverse coherence length up to  $250 \mu\text{m}$ ) available at SR imaging setups—allows us to obtain contrast between materials as soon as there is a difference in electron density. This additional information is crucial whenever one is interested in separating materials which have very similar linear attenuation coefficients such as Al and Si in the present case.

By absorption and holographic imaging we investigated samples representing early foaming stages<sup>18</sup> which stem from different precursor materials. In particular, here we present one sample compacted by extrusion from a powder mix of a prealloyed AA6061 metal powder and a blowing agent (0.5 wt %  $\text{TiH}_2$ ). Further two samples representing two different expansion stages are composed of two elemental powders (93 wt % Al+7 wt % Si) mixed with the same blowing agent but compacted by closed-die uniaxial compression.<sup>19</sup>

Figures 2(a), 2(b), and 2(d) show high-resolution absorption-contrast tomographic slices of the three samples. During heat treatment of the foamable precursor, isolated cracks have appeared due to the hydrogen released by the blowing agent. In later stages (not investigated here), these cracks would first form open-porous crack networks,<sup>10</sup> and then transform to the typical closed-cell foam structures studied intensely elsewhere (see, e.g., Ref. 8).

As we are interested in the pore initiation process we perform a numerical analysis<sup>16</sup> on the segmented tomographic 3D data sets which is based on *erosion* (see, e.g., Ref. 17), a morphological image processing technique. In order to assure comparability, the 3D data sets—obtained with the same experimental parameters—have been treated with the same image processing parameters. The 3D correlation properties between the positions of  $\text{TiH}_2$  blowing agent particles and pores are reflected by profiles of  $\text{TiH}_2$  concentration (see Fig. 3) as a function of increasing distance from the pore space which is parametrized by the volume of the eroded solid matrix. For instance, a more or less constant value is a sign for a random distribution while positive or negative slopes of the profile indicate anticorrelation or correlation, respectively.

From Fig. 3(a), a significantly different behavior can be observed for the two precursor materials at early foaming

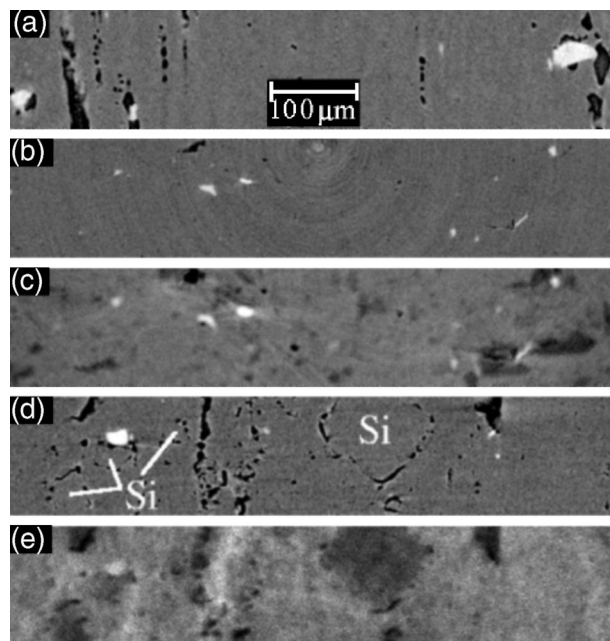


FIG. 2. Reconstructed cross-sectional images through partly expanded foam samples. (a) AA6061 (porosity  $P=2.7\%$ ); (b) and (c) AlSi7 ( $P=0.12\%$ ); (d) and (e) AlSi7 ( $P=4.9\%$ ) Pores are rendered black, the blowing agent  $\text{TiH}_2$  white. (a), (b), and (d) are absorption contrast images, (c) and (e) holographic images. Image widths are 512 pixels of  $1.4 \mu\text{m}$  size in all cases.

stages: AA6061 with a porosity<sup>18</sup> of  $P=2.7\%$  exhibits a very strong spatial correlation with up to 2.5 times the average concentration near the pores, whereas for AlSi7 with  $P=4.9\%$  no significant spatial correlation between pores and blowing agent is found (normalized concentration values near unity)—only later, for more progressed expansion stages (not shown here), a significant correlation appears, agreeing with 2D scanning electron microscopy (SEM) observations<sup>11</sup> of an AlSi7 sample.

The high imaging resolution (reflected by a pixel size of  $1.4 \mu\text{m}$ ) allows us to perceive characteristic differences in shape and arrangement of cracks between the two alloys, see Figs. 2(a) and 2(d): For AA6061 (a) the cracks are preferably oriented in the up-down direction (parallel to extrusion direction) while AlSi7 (d) exhibits angular or curved cracks in the shown slices. An explanation for both the dif-

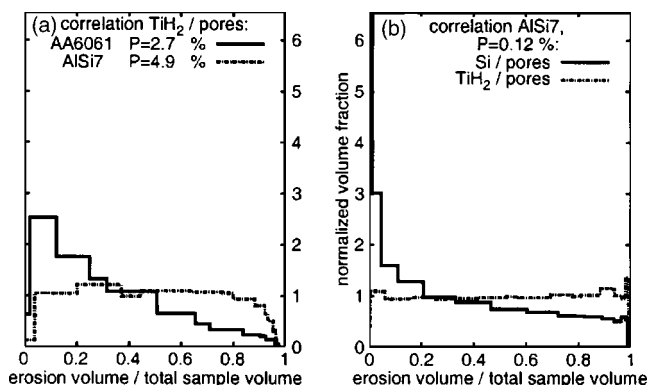


FIG. 3. Spatial correlation between pores and powder particles investigated with  $1.4 \mu\text{m}$  voxel size. Plotted are volume fractions of  $\text{TiH}_2$  [(a) all and (b) dashed lines] and Si [(b) full line], normalized to their mean volume fractions, with increasing distance (parametrized by the erosion volume of the solid matrix) around the pores. The computations were carried out on 3D data sets of  $660^3$  voxels.

ferent crack shapes and the different correlation between  $\text{TiH}_2$  and pores in the two alloys can be obtained by phase-contrast imaging employing the partial coherence of the SR imaging setup.

Due to different electron densities of Al and Si, the Si particles differ from the Al matrix in the holographically reconstructed images [Figs. 2(c) and 2(e)] and appear as dark gray, edged particles whereas in the corresponding absorption images [Figs. 2(b) and 2(d)] they cannot be distinguished from the surrounding matrix. Therefore, the holographic reconstruction allows us to label regions in the absorption contrast tomographs as “Al” and “Si” although there is no contrast discernible between these regions in Fig. 2(d). After this labeling we observe that cracks are predominantly aligned around silicon particles in the AlSi7 material, explaining the observed angular or curved shapes in the absorption images. This indicates a mechanism of crack initiation which is alternative to pore generation around blowing agent particles. These results confirm previous observations in 2D surface studies by SEM (Ref. 11) which gave first evidence for this mechanism now extended to nondestructive 3D imaging of the sample volume.

Having identified the silicon particles we incorporate this information into the numerical 3D correlation analysis. Due to image noise, analysis of the later foaming stage of AlSi7 ( $P=4.9\%$ ) is rather difficult. Especially for very early foaming stages ( $P=0.12\%$ ), however, we can show the presence of a strong spatial correlation [see Fig. 3(b)] between crack positions and silicon particle positions. This perfectly agrees with the observation of crack formation at the Al/Si interfaces in the tomographic images. Although the results concerning the correlation Si/pores cannot be compared quantitatively<sup>20</sup> to the correlation  $\text{TiH}_2$ /pores a clear qualitative statement concerning the high correlation Si/pores is allowed.

These results in combination with the comparison of (d) and (e) of Fig. 2 enable us to conclude that for the powder compact the bonding strength between Si and Al is lower than between Al and  $\text{TiH}_2$  or between individual Al particles. Pores thus initiate at Al/Si interfaces by mechanical cracking during gas release triggered by the heating process. It has to be assumed that the evolving hydrogen gas migrates from the  $\text{TiH}_2$  particles to the Al/Si interfaces, probably along boundaries between former powder particles to create cracks there. It seems that in very early stages this is the dominant mechanism of porecrack formation, explaining why in such Al-Si two-powder compacts no significant correlation between pore initiation and the blowing agent particle sites is found.

Synchrotron-radiation tomography allowed us to study nondestructively early stages of metal foam formation.

Monochromatic radiation facilitated the distinction between pores, alloy matrix, and blowing agent. 3D image processing and analysis techniques were developed and applied to the quantitative determination of the spatial correlation between pores and blowing agent. Significantly different correlation properties were found for AA6061 and AlSi7 precursor materials which, by holographic imaging, could be interpreted as specific crack initiation at the Al/Si interface in early foaming stages for the latter precursor material.

Support by the Deutsche Forschungsgemeinschaft (Ba 1170/4–2) and the Arbeitsgemeinschaft Industrieller Forschungsvereinigungen (KF 0010502KWM9) are gratefully acknowledged.

<sup>1</sup>M. Ashby, A. Evans, N. Fleck, L. Gibson, J. Hutchinson, and H. Wadley, *Metal foams: A Design Guide* (Butterworth-Heinemann, Oxford, 2000).

<sup>2</sup>J. Banhart, *Prog. Mater. Sci.* **46**, 559 (2001).

<sup>3</sup>Metalfoam.net web site: Url <http://www.metalfoam.net/>

<sup>4</sup>F. Baumgärtner, I. Duarte, and J. Banhart, *Adv. Eng. Mater.* **2**, 168 (2000).

<sup>5</sup>J. Banhart, H. Stanzick, L. Helfen, and T. Baumbach, *Appl. Phys. Lett.* **78**, 1152 (2001).

<sup>6</sup>J. Banhart, H. Stanzick, L. Helfen, T. Baumbach, and K. Nijhof, *Adv. Eng. Mater.* **3**, 407 (2001).

<sup>7</sup>H. Bart-Smith, A.-F. Bastawros, D. Mumm, A. Evans, D. Sypeck, and H. Wadley, *Acta Mater.* **46**, 3582 (1998).

<sup>8</sup>O. Olurin, M. Arnold, C. Körner, and R. Singer, *Mater. Sci. Eng., A* **328**, 334 (2002).

<sup>9</sup>J. Banhart, D. Bellmann, and H. Clemens, *Acta Mater.* **49**, 3409 (2001).

<sup>10</sup>L. Helfen, T. Baumbach, H. Stanzick, J. Banhart, A. Elmoutaouakkil, and P. Cloetens, *Adv. Eng. Mater.* **4**, 808 (2002).

<sup>11</sup>U. Mosler, A. Müller, H. Baum, U. Martin, and H. Oettel, in *Cellular Metals and Metal Foaming Technology*, edited by J. Banhart, M. Ashby, and N. Fleck (MIT-Verlag, Bremen, Germany, 2001), pp. 233–238.

<sup>12</sup>P. Cloetens, M. Pateyron-Salomé, J. Y. Buffière, G. Peix, J. Baruchel, F. Peyrin, and M. Schlenker, *J. Appl. Phys.* **81**, 5878 (1997).

<sup>13</sup>J. Kinney, N. Lane, and D. Haupt, *J. Bone Miner. Res.* **10**, 264 (1995).

<sup>14</sup>P. Cloetens, W. Ludwig, E. Boller, L. Helfen, L. Salvo, R. Mache, and M. Schlenker, in *Proceedings SPIE: Developments in X-Ray Tomography III*, edited by U. Bonse (SPIE, San Diego, CA, 2002), Vol. 4503, pp. 82–91.

<sup>15</sup>P. Cloetens, W. Ludwig, J. Baruchel, D. van Dyck, J. van Landuyt, J. Guigay, and M. Schlenker, *Appl. Phys. Lett.* **75**, 2912 (1999).

<sup>16</sup>L. Helfen, H. Stanzick, J. Ohser, K. Schladitz, P. Pernot, J. Banhart, and T. Baumbach, in *Proceedings SPIE: Testing, Reliability, and Application of Micro- and Nanomaterial Systems*, edited by N. Meyendorf, G. Baaklini, and B. Michel (SPIE, San Diego, CA, 2003), Vol. 5045, pp. 254–265.

<sup>17</sup>K. Castleman, *Digital Image Processing* (Prentice-Hall, Englewood Cliffs, New Jersey, 1996).

<sup>18</sup>For classification of foam expansion stages, the porosity  $P=V_{\text{pores}}/V_{\text{total}}$  is used where by analysis of 3D images of size  $V_{\text{total}}$  the volumes of the segmented pore space  $V_{\text{pores}}$  are determined.

<sup>19</sup>Al-Si alloys are technologically favorable due to their low melting point. Using two elementary base powders enables an especially cost-efficient production.

<sup>20</sup>Naturally, the parameters of image processing have to be adapted to the images. Moreover, image blurring (as slightly discernible from Fig. 2 in the comparison between the holographic and the absorption images) usually results in blurred correlation profiles.